ENCLOSURE 2

MFN 15-040

Response to Request for Additional Information Regarding Review of Licensing Topical Report NEDE-33798P, "Application of NSF to GNF Fuel Channel Designs"

Non-Proprietary Information – Class I (Public)

IMPORTANT NOTICE

This is a non-proprietary version of Enclosure 1, from which the proprietary information has been removed. Portions of the enclosure that have been removed are indicated by an open and closed bracket as shown here [[ ]].

RAI-1 NSF Alloy Composition

Section 2.2 of NEDE-33798P defines the nominal composition and allowable ranges of major alloying elements. Current practice is to define nominal along with a tight range for manufacturing tolerance. While the American Society for Testing and Materials allows a broader range, it also comes with required periodic testing. Further justification is required for the proposed ranges.

Response:

The range in composition of NSF defined in the Licensing Topical Report (LTR) is analogous to the composition ranges defined for Zircaloy-2 (Zry-2) and Zircaloy-4 (Zry-4) in ASTM B352/352M-11. As suggested above, the standard practice is to tighten the chemistry ranges when purchasing a material. But chemistry is not the only material specification. Typically, there is a microstructure requirement (fully recrystallized in the case of NSF), mechanical property requirements and corrosion performance requirements. Similar to the requirements in ASTM B352/352M-11 and as defined in 10 CFR 50 Appendix B, for the material to be accepted, the supplier is required to provide test results in quality documents that provide objective evidence that the material lot meets all requirements.

a) With respect to corrosion rates, a similar Zr-Nb-Sn-Fe alloy shows dramatic differences between 1.2 percent - 0.6 percent Sn. This is contrary to a portion of your justification. Please describe the influence of Sn on the expected corrosion of NSF channels within the proposed ranges.

Response:

For NSF, Global Nuclear Fuel (GNF) considers the range of Sn to be from [[ ]] Sn.

It is expected that alloy chemistry will be one source of variability in corrosion performance. Based on the data presented and the references provided in the LTR, the variability in corrosion rates with differences in Sn is acceptable. Besides the corrosion data in Figure 2-12 (updated in response to RAI-3(d)), Nikulina et al. (LTR Reference 15) found the corrosion performance was adequate for E635 with Sn levels between 1.2% and 1.3%. In LTR Reference 23, Comstock et al. found Pressurized Water Reactor (PWR) corrosion improved in ZIRLO when the Sn decreased from 1.2% to 0.97%. The suggestion of a strong negative effect on corrosion as a function of Sn in the [[ ]] range cannot be evaluated without the specific reference information.

However, it is also important to note that the impact of corrosion on channel performance is on metal thinning that is accounted for in the mechanical design process (LTR Reference 1). As discussed in Section 2.10, metal thinning accounts for corrosion on both sides of the channel over its entire length. When accounting for the effect of metal thinning in the channel design

process, it is assumed that the channel thickness is decreased over the entire channel length by the design curve provided in Figure 2-12. Thus, it is more appropriate to think of the corrosion thickness value in Equations 2-31 and 2-32 as nominal values rather than maximum values in a distribution. The implication of this is that the average corrosion thickness must remain below the design curve rather than every local area remaining below the design curve.

With this understanding and given the significant margin between the measured nominal corrosion value of NSF and the design value (see updated figure in response to RAI-3(d)), it is expected that this margin will cover all variation in nominal corrosion on future NSF channels caused by variation in ingot chemistry or from other variables such as location on the channels.

b) Section 2.2.3 provides no discussion of the potential effect of alloying composition on shadow corrosion. On a similar note, there is no discussion on hydrogen uptake. Please describe the influence of alloying composition on hydrogen uptake and shadow corrosion induced bow.

Response:

Shadow corrosion and hydrogen uptake are important because they are the key variables in shadow corrosion-induced bow. Hydrogen uptake is discussed in more detail in the response to RAI-3. An updated version of the shadow bow data for NSF is provided in the response to RAI-9. The GNF plan is to evaluate the variability in shadow bow directly (and thus shadow corrosion and hydrogen pickup indirectly) by measuring channel distortion in the NSF channels that are part of the 8% Lead Use Channel (LUC) program (See Reference 10-1 of this RAI). Specifically, approximately 225 channels will be measured as part of that program and will adequately quantify the variability in shadow bow of NSF (including the effects of variation in alloy chemistry and processing). These measurements are part of the future Post Irradiation Surveillance plan discussed in the response to RAI-10(a).

c) According to Table 2-1, the nominal composition of NSF includes 1.0 percent Sn, and 0.12 percent O. GNF provided strength data for a nominal composition. In the Licensing Topical report (LTR) for Ziron cladding, GNF indicated that the YS and UTS for Ziron cladding was likely [[
]] Table 2-2 of NEDE-33798P lists an allowable minimum content of [[
]] Sn and [[ ]] O.

i. Describe the impact of these minimum ranges of Sn and O on TS and UTS.

ii. Describe the impact of these minimum ranges of Sn and O on creep rate and channel bulge calculations.

iii. Describe the impact of these minimum ranges of Sn and O on maximum channel distortion predictions (bow and bulge).

iv. Identify any post-irradiated data from NSF lead channels at these lower ranges.

Response:

i. As stated in the LTR in Section 2.8.1, the design strength of NSF or any zirconium alloy is actually controlled in the material specification that requires objective evidence that the material lots meet the strength requirements. This accounts for any variability in the material strength from variation in chemistry.

ii. There is open literature evidence (Nikulina et al., LTR Reference 15) that the in-reactor creep rate of NSF-like alloys is lower than other Zirconium (Zr) alloys. However, the test conditions considered by Nikulina et al. were more similar to fuel rod performance in PWR-type conditions (~330^{o}C and ~120 MPa/~17 ksi) than in Boiling Water Reactor (BWR) channels. While stress concentration sites exist in the channel and can cause the stress levels to be in the [[ ]] psi range, the uniform tensile stress due to the pressure drop across the channel face is calculated to be less than [[ ]] psi for a 10 psi pressure drop. GNF has observed [[

]]

This point was made in the LTR in Section 2.9.1, where it was discussed that the stress levels in the channel are in the [[

]].

The conclusion from this analysis is that the variation in Sn and O within the range of NSF will have no significant effect on channel bulge calculations.

iii. The effect of variability in Sn and O content on bulge was discussed above for creep deformation. However, there is also an elastic component for bulge. The case is made in Section 2.3 of the LTR that the elastic properties of NSF will not vary significantly with alloy content. Thus, both creep and elastic bulge are not affected by variation in Sn and O content.

The impact of variability in Sn and O on channel bow is expected to be [[ ]]. The effect of Sn on irradiation growth that causes fluence bow was discussed in Section 2.11. Variation in Sn has [[ ]]. In alloys such as NSF, the role of Sn may be to [[

]]. Oxygen is not known to have a significant impact on irradiation growth in zirconium alloys. The impact of Sn and O on shadow corrosion, which causes shadow bow, is discussed above in part (b) of this Request for Additional Information (RAI), and will effectively be evaluated by channel bow measurements.

Ultimately, the purpose of the 8% LUC program (MFN 12-074 Supplement 2-A – Reference 1-1) is to explicitly address the potential effects of material and fabrication variability on performance. After these partial reloads are discharged, GNF will perform inspections to measure both channel bulge and bow to better quantify the effects of not only varying chemistry but also variations in vendor processing.

iv. The variation in chemistry for the discharged NSF channels is limited because these were the first channels manufactured. Specifically the range of Sn in these channels is from [[ ]]wt%. When considering all the NSF channels manufactured from 2000 to 2014, the Sn has varied from [[ ]]wt%. As discussed above the purpose of the 8% LUC program is to address potential variations in chemistry.

Reference

1-1 Letter from A.A. Lingenfelter (GNF) to Document Control Desk (US NRC), Subject: Accepted Version of Enhanced Lead Use Channel (LUC) Program for NSF Fuel Bundle Channels, MFN 12-074 Supplement 2-A, April 15, 2013.

RAI-2 Range of Applicability

Section 4 of NEDE-33798P is titled "Applicability." Besides the discussion of allowable range of alloying elements in Section 2.2.3 of NEDE-33798P, there is no attempt to define a range of applicability of NSF material to GNF channel designs. Are further limitations necessary based on the extent of in-reactor experience and empirical database? For example, is a limit on residence time, neutron fluence (or equivalent fuel burnup), and/or effective control blade exposure (ECBE) necessary?

Response

[[

]], it is more appropriate to consider a fluence limit for NSF channels. Based on the available irradiation growth data that shows NSF is resistant to breakaway growth for fluences up to 2.2E22 n/cm^2, a reasonable fluence limit for NSF channels is 2.0E22 n/cm^2 (calculated as the average for the channel). Using the correlation between fluence and exposure reported in the response to RAI-5, this fluence corresponds to a bundle exposure of ~[[ ]]; thus, the expected average channel fluence at [[ ]]. Therefore, the applicability range of the NSF channel will be based on only residence time and will specifically be limited to [[ ]] years. As of March 2015, four NSF channels have operated for four two-year cycles.

GNF recognizes the potential value of extending the current residence time limits or to re-use channels. Any potential re-use of NSF channels or operation of NSF channels beyond the current residence time limits would follow the current GESTAR requirements for lead-test assemblies. In addition, if a channel accumulates more than [[ ]] inch-days of Effective Control Blade Exposure (ECBE) during a cycle, it will be treated as a lead-test assembly if reinserted in a rodded location (i.e., a cell with a control rod). The lead test limitations would apply until sufficient evidence is collected to support the extension of the applicability range of NSF channels, which would be documented and submitted to the NRC for information.

RAI-3 Hydrogen Pickup and Corrosion

Figures 2-12 and 2-20 of NEDC-33798P provide measured oxide thickness and absorbed hydrogen for NSF and Zry-2 channels.

a) Does GNF have experience with Zry-4 channels? If so, describe the relationship between Zry-4 and NSF channels with respect to oxidation and hydrogen absorption.

Response:

Yes, GNF does have experience with Zircaloy-4 channels. Zircaloy-4 was used as the channel material prior to transition to Zircaloy-2 in 1990s. Zircaloy-4 has also been used in some more recent applications as an interim measure to mitigate the shadow-corrosion induced channel bow issue. GNF's experience with Zircaloy-4 channels is found in paper #8078 in the 2008 Water Reactor Fuel Performance Meeting (WRFPM) in Seoul, Korea. The main advantage of Zircaloy-4 (relative to Zircaloy-2) is the low hydrogen pickup fraction, typically around 10% (see, for example, Miyashita et al. in the 2007 Light Water Reactor Fuel Performance Meeting (LWRFPM) in San Francisco). A comparison of NSF corrosion relative to Zircaloy-4 (and Zircaloy-2) has been provided in GNF's paper at the 2013 LWRFPM (paper #8465). The tabulated results are reproduced below in Table 3a-1. (Note the average results for NSF and Zircaloy-2 are shown in Figure 2-12 and also in RAI-3(d).

Table 3a-1 also includes hydrogen data that are shown in Figure 2-20 of the LTR (for NSF and Zircaloy-2). It should be noted that the Zircaloy-4 data were obtained from a channel that was discharged after 4.3 years with a fuel assembly burnup of 33.4 GWd/MTU, and are being compared to NSF data with ~49 GWd/MTU burnup after 5.83 years. It can be seen from the data that in-reactor corrosion performance of the NSF channel is superior to Zircaloy-4 that has seen less time and neutron exposure. The hydrogen pickup fraction of NSF is [[ ]]. For NSF, the data below correspond to an average pickup fraction of ~[[ ]]%, and, when additional data is included, an average pickup fraction of ~[[ ]]% is obtained (see also RAI-3(d)). These values are [[ ]] or ~10% reported by Miyashita.

Table 3a-1

Channel Material (GWd/MTU) [inch-days]	Elevation (in)	Non-Blade Side			Blade Side		
		Outer Surface (μm)	Inner Surface (μm)	Metal Hydrogen (ppm)	Outer Surface (μm)	Inner Surface (mm)	Metal Hydrogen (ppm)
Zry-2	120	10.2	14.6	[[	9.1	16.7	[[
(49.2)	90	9.5	14.5		13.4	18.1	
[4,222]	55	9.5	14.4		9.1	17.2	
	20	9.9	5.9		4.7	10.7	
	Average	10	12		9	16	
NSF	120	22.8	36.4		19.1	34.4	
(49.1)	90	22.6	34.9		24.7	38.4	
[4,222]	55	27.6	33.2		30.7	27.7	
	20	11.7	18.6		19.7	18.3	
	Average	21	31		24	30	
Zry-4	120	33	44		35	46	
(33.4)	90	32	53		43	60	
[30,896]	55	37	49		42	51	
	20	32	38		43	35	
	Average	34	46	]]	41	48	]]

b) Figure 2-12 shows a single data point and one standard deviation for NSF corrosion. The NSF data point sits just above the maximum corrosion data point for Zry-2. Beneath the NSF data point is a Zry-2 data point, i.e., at the same exposure time (~5.83 years).

i. Describe the basis (e.g., local maximum, average) of the Zry2 Design Upper Bound curve, which is given by equations 2-32, 2-33 and 2-34 in the LTR.

ii. Describe the relationship (i.e., irradiation conditions, fluence) between the NSF data point and the Zry-2 data points around ~5.83 years.

Response:

i. Equations 2-31, 2-32, 2-33 and 2-34 together form the basis for defining the design upper bound line in Figure 2-12. As stated in Section 2.10 of the submitted LTR, the design upper bound line for Zircaloy-2 is used in GNF's channel mechanical design process to assess the maximum amount of metal thinning due to nominal corrosion in order to preserve mechanical integrity of the channel. Although the equations are written in the form of upper bound corrosion as a function of time, the channel design in practice considers only the maximum residence time ([[ ]]). The intent of the equations is therefore not focused on predicting the corrosion oxide thickness, but to provide the expected maximum amount of metal thinning that needs to be accounted for

due to corrosion up to end of life. In Section 2.10, Equations 2-31 to 2-34 are stated for completeness to show how the maximum value at any given time can be derived. The equations merely reflect the fact that irradiation effect (Equation 2-34) dominates and that there is a minor contribution due to thermal exposure. Given the purpose of the design upper bound line, the reason for Figure 2-12 is not to demonstrate any agreement between the line and measured data points; instead, the purpose is to demonstrate oxide thickness measurements fall below the design line, or more strictly, the value at maximum residence time.

ii. The NSF data point in Figure 2-12 represents the average, and associated standard deviation, of all oxide measurements taken from one NSF channel that had operated for three two-year cycles in a US plant reaching ~49 GWd/MTU fuel assembly burnup in 5.83 years. During its operation, the channel had an ECBE of 4,222 inch-days, which is relatively low, such that significant corrosion enhancement due to the shadow corrosion mechanism is not expected. Coupons from four axial elevations (20, 55, 90 and 120 inches) of the NSF channel were measured as part of the hot cell examination. The Zircaloy-2 data point in Figure 2-12 represents the corresponding measurements made on a Zircaloy-2 channel that operated in symmetric core locations to the NSF channel during all three cycles of operations. The residence time, fuel assembly burnup and ECBE therefore match those for the NSF channel. For hot cell examination, coupons from the same four axial elevations (20, 55, 90 and 120 inches) were measured. For each examined axial elevation, the fluence level for Zircaloy-2 therefore matches that for NSF. See also RAI-3(a) for a detailed breakdown of measured oxide thickness.

c) Figure 2-20 shows hydrogen absorption as a function of hydrogen generated for a NSF channel and a Zry-2 channel operated in symmetric core locations.

i. Describe the higher hydrogen generated in the NSF channel.

ii. Describe how hydrogen absorption is affected by duty, fluence, and water chemistry (e.g., HWC, NMCA, OLNM).

iii. Identify any differences between operations of these two channels (e.g., ECBE).

Response:

i. In Figure 2-20 (and in an updated version in Figure 3d-2 below), the "Hydrogen Generated" parameter is the theoretical potential value of the hydrogen generated from the corrosion reaction with water on both inside and outside channel surfaces expressed as a hydrogen content in the remaining metal, assuming it is uniformly distributed in the channel wall. In other words, the parameter represents the potential hydrogen content if the material were to have a 100% hydrogen pickup value. The parameter is related to the combined (inside and outside) oxide thickness and the metal thickness. Figure 2-20 in the LTR shows data for a pair of NSF and Zircaloy-2 channels that have

the same mechanical (dimensional) design and operated for 5.83 years (three two-year cycles) in symmetric core locations and hence have the same operational history. The higher values of "Hydrogen Generated" for NSF merely reflect the higher corrosion rate of NSF compared with Zircaloy-2, as shown by the pair of points at 5.83 years in Figure 2-12. Therefore, this is best characterized as higher hydrogen generated **by** the NSF rather than absorbed **in** the NSF.

ii. For non-heat transfer zirconium-alloy components, time and fast neutron fluence are usually considered to be the two primary factors that could affect hydrogen absorption in a given alloy. Duty, in the context of how a channeled assembly is operated, therefore is a potential factor in affecting time to achieve a particular level of fluence. This is true mostly for Zircaloy-2 for which there can be considerable variation in hydrogen pickup fraction at moderate to high fluence levels or residence times. In contrast, Zircaloy-4 typically shows low hydrogen pickup fraction regardless of fluence or time; however, the corrosion is considerably greater than Zircaloy-2. For NSF, [[

]]. Figure 2-20 in the submitted LTR provides a direct comparison between NSF and Zircaloy-2. The figure shows that NSF had greater amounts of corrosion, as reflected by higher "Hydrogen Generated" values; however, [[

]]. As discussed below in RAI-3(d), there has been another set of hot cell data. The differentiating feature for the second set of hot cell data is the very high control blade exposure experienced by the channel (ECBE 51,262 inch-days). As shown in the measured versus expected hydrogen plot in RAI-3(d), data for NSF from both hot cell campaigns form one population, sharing a common slope reflecting [[ ]]. As control blade exposure is the main duty parameter of interest for channels, the updated results presented in RAI-3(d) show that hydrogen pickup of NSF is not sensitive to variations in this key duty parameter.

Under BWR conditions, available information on Zircaloy-2 does not show appreciable variations that can be assigned to variations in water chemistry (e.g., Hydrogen Water Chemistry (HWC), Noble Metals Chemical Addition (NMCA) or On-Line NobleChem^{TM} (OLNC)). Specific to NSF, all channels that were deployed in the United States (US) under LUC or expanded LUC programs have operated under HWC with zinc injection and with either NMCA or OLNC water chemistry conditions. Difference in hydrogen pickup behavior of NSF due to NMCA versus OLNC is not expected and is supported by hot cell examination results. As discussed in RAI-3(d), there have been two hot cell campaigns. The first is for a channel that operated under NMCA for all three cycles. The second is for a channel that operated under NMCA in the first cycle and then operated under OLNC in the second and third cycles. The hot

cell results after three cycles of operation showed [[
]].

iii. There is no appreciable difference between the two channels, both operated for 5.83 years (three two-year cycles) in symmetric core locations reaching ~49 GWd/MTU with an ECBE of 4,222 inch-days.

d) Please provide any data for NSF oxidation and hydrogen uptake taken since this topical report was submitted.

Response:

Since the submittal of the LTR, there has been another set of hot cell examination providing corrosion and hydrogen uptake data for NSF channels. The first set of data (shown in the submitted LTR) is from the 65 mil portion of a NSF channel that operated for three two-year cycles (5.83 years) reaching ~49 GWd/MTU burnup with a relatively low ECBE value of 4,222 inch-days. The newer, second set is from the 75 mil portion of a NSF channel that operated also for three two-year cycles (5.53 years) reaching ~40 GWd/MTU burnup with a very high ECBE value of 51,262 inch-days. Updated Figures 2-12 and 2-20 are presented below. The data in Figure 3d-1 are tabulated in Table 3d-1 with the channel exposure and ECBE value of each point. Note that data from the companion Zircaloy-2 channel that operated in the symmetric core location to the NSF channel was collected only during the first hot cell campaign (5.83 years of operation). For the hydrogen pickup plot (Figure 3d-2), the theoretical hydrogen generated values takes into consideration the oxide thickness on both inside and outside surfaces as well as the channel thickness – see also RAI-3(c)(i). Compared with Figure 2-20 in the submitted LTR, it can be seen from the revised plot that inclusion of additional data for NSF yielded essentially the same average pickup fraction (slope) for NSF.

[[

]]

Figure 3d-1 Upper Bound Design Value for Corrosion and Recent Hot Cell Oxide Thickness Data for Zircaloy-2 and NSF
(Uncertainty bars represent one standard deviation)

[[

]]

[[ ]]

Figure 3d-2 Measured Versus Expected Hydrogen Pickup
(There are two sets data for NSF and one set for Zircaloy-2)

Table 3d-1 Operational Conditions of Measured Channel Oxide Thickness in Figure 3d-1

Channel Material	Assembly Exposure	Time	ECBE	Average Oxide	StDev
	(GWd/MTU)	year	inch-days	microns	
Zircaloy-2	39.7	4.07	8,133	[[	
	36.5	4.07	10,721		
	39.6	4.07	21,916		
	40.7	4.07	16,216		
	48.2	5.16	14,025		
	47.9	5.16	0		
	48.1	5.70	27,112		
	48.1	5.70	27,112		
	19.7	1.86	34,105		
	43.9	6.58	17,795		
	42.9	6.58	712		
	49.3	5.83	4,222		
NSF	49.2	5.83	4,222		
	40.3	5.53	51,262		]]

e) In MFN 12-074, GNF states, "The measured oxide thickness of NSF after [[ ]] For comparison, the measured oxide thickness of Zircaloy-2 channels after [[ ]]."

The statement appears to refer to the data expressed in the following figure and table:

[[

TABLE I. Oxide Thickness Measurements of Zircaloy-2, NSF and Zircaloy-4 Channels

Channel Material (GWd/MTU) [inch-days]	Elevation (in/mm)	Non-Blade Side		Blade Side	
		Outer Surface (μm)	Inner Surface (μm)	Outer Surface (μm)	Inner Surface (μm)
Zr-2	120/3048	10.2	14.6	9.1	16.7
(49.2)	90/2286	9.5	14.5	13.4	18.1
[4222]	55/1397	9.5	14.4	9.1	17.2
	20/508	9.9	5.9	4.7	10.7
	Ave.	10	12	9	16
NSF	120/3048	22.8	36.4	19.1	34.4
(49.1)	90/2286	22.6	34.9	24.7	38.4
[4222]	55/1397	27.6	33.2	30.7	27.7
	20/508	11.7	18.6	19.7	18.3
	Ave.	21	31	24	30

]]

Figure. MFN 12-134, p. 77 (78 of 82 in pdf)

(Table I., Paul E. Cantonwine, Yang-Pi Lin, Dan R. Lutz, David W. White, and Kevin L. Ledford, "BWR Corrosion Experience on NSF Channels," Paper 8465, Topfuel 2013, Charlotte, September 15-19, 2013.)

i. The oxidation rate for NSF seems to be a factor of 2 or 3 times that of Zry-2. Are these results obtained under the same irradiation conditions and duty level? What is the expected corrosion thickness after 8 years of operation?

ii. GNF measurements indicate that the inside oxide thickness is greater than the outside thickness. In Equation 2-31 (LTR), what corrosion thickness is used – inside or outside?

Response:

i. In Figure 2-12, the data for NSF and Zircaloy-2 at 5.83 years are obtained from channels on assemblies that operated for three two-year cycles in symmetric core locations and hence have equivalent irradiation condition and duty level – also see the response to RAI-3(b). As discussed in RAI-3(b), the Design Upper Bound line in Figure 2-12 is used in GNF's channel mechanical design process to assess the maximum amount of metal thinning due to corrosion. [[
]]. As discussed in the response to RAI-1, this upper bound value should be compared to the nominal measured value. Given the margin between the upper bound value and the nominal measured value of NSF corrosion, the Design Upper Bound line is adequate for metal thinning calculations. Based on extrapolation of the corrosion data in the LTR and the response to RAI-3(d), the nominal corrosion thickness of NSF at [[ ]] years would be around [[ ]] microns. Four NSF channels (two each in two plants in the US) have

operated for four two-year cycles. All four channels completed ~eight years of operations without known issues.

ii. Equation 2-31 does not make a differentiation between the inside or outside surface. It assumed both sides to be the same, as shown by the inclusion of the factor of two in the equation. As stated in (i) above, the intent of the equation is not so much to predict the thickness of the corrosion oxide; rather, the intent is to provide a guidance to the expected maximum amount of metal thinning due to corrosion. To satisfy this purpose, the expected behavior for NSF is to show corrosion less than assumed in Equation 2-31 and associated Equations 2-32 through 2-34 – also see the response to RAI-3(b).

f) The LTR does not address high temperature corrosion for NSF channels under accident conditions.

i. Describe the expected peak channel temperature history during the limiting Boiling Water Reactor (BWR) Loss of Coolant Accident (LOCA).

ii. Describe the predicted corrosion and channel performance under these conditions.

iii. Provide weight gain vs time for NSF and Zry-2 material (see Figure B-15 of NEDC-33353P, Revision 0) for the above conditions, or 1000°C.

Response:

i) During a LOCA scenario, the channel acts as a heat sink in assisting removal of decay heat from the fuel assembly. The channel temperature will therefore increase as more heat is absorbed. The increase in channel temperature will lag behind the cladding temperature of the adjacent fuel rods located at the periphery of the fuel assembly. Ultimately, the temperature of the channel would approach that of the adjacent rods facing the channel. The temperature reached by the channel will be, however, lower than the limiting fuel rod peak clad temperature, which comes from fuel rods in the interior of the fuel assembly having less effective heat removal compared with peripheral rods.

ii) NSF contains >~97 % (by weight) of zirconium. The corrosion or reaction of steam will therefore be dominated by the zirconium-water reaction. Although alloying elements can modify the steam oxidation process somewhat, a major departure from typical zirconium-alloy behavior is not anticipated. From a review of the literature (NUREG/CR-6967), it is noted that steam oxidation kinetics for Zirlo, which has a similar composition as NSF (except for Fe), essentially follow the Cathcart-Pawel (CP) relationship at 1,000, 1,100 and 1,200^{o}C. The oxidation behavior of NSF at 1,000^{o}C as discussed in (iii) is [[

]].

For zirconium alloys at elevated temperatures, the main embrittlement mechanisms are metal thinning due to oxidation, oxygen embrittlement and hydrogen embrittlement. The

impact of metal thinning due to oxidation, including the effect of dissolved oxygen ahead of the oxide layer, will depend on the metal thickness. For fuel cladding, the degree of zirconium-alloy embrittlement is typically expressed in terms of Equivalent Cladding Reacted (ECR) that takes into account oxide thickness, cladding thickness and thickness of the oxygen embrittled layer. When applied to NSF channels, for a given amount of oxidation and hence oxygen embrittled layer (as predicted by the CP relationship), the overall equivalent channel reacted would be lower on account of the greater channel thickness compared with the cladding case. In addition, as discussed in (i), the peak channel temperature would be lower than the Peak Cladding Temperature (PCT). The ECR for the channel next to the fuel assembly with the limiting PCT (and hence ECR) would be lowered further compared with the limiting ECR on account of the peak temperature difference. With regard to absorbed hydrogen, the thicker channel compared with cladding means that channels will be more tolerant of hydrogen. The effect of absorbed hydrogen during the transient is typically not considered, except near 1,000^{o}C when some zirconium alloys can develop early onset of breakaway oxidation with associated increased hydrogen absorption.

iii) High temperature steam oxidation tests were obtained for Zircaloy-2 and NSF channel strip in the bare (initially unoxidized) condition and for NSF channel [[

]]. The tests were performed at 1,000^{o}C for various times ranging from 500 seconds to 7,000 seconds. Results are compared in Figure 3f-1 to the CP relationship for times less than breakaway. [[

]].

[[

]]

Figure 3f-1 Measured Weight Gain of NSF Compared to Zircaloy-2 During a High Temperature Oxidation Test for Simulating LOCA Conditions

RAI-4 Channel bow, creep and oxidation

a) MFN 12-134 provided significant background for the NSF channel performance. The shadow corrosion-induced bow data for NSF channels is limited relative to the Zry-2 data presented on page 75. Please provide this figure with only the NSF LUC data compared to the Zry-2 control channels that operated under similar conditions to the NSF channels.

Response:

The shadow corrosion-induced bow data for NSF is compared in the figure below to counterpart Zircaloy-2 control channels that operated during the same plant and cycle and with the same control history as the NSF channels. In this small population, it is apparent [[

]].

[[

]]

Figure 4a-1 Inferred Shadow Bow of NSF LUCs Compared to the Zircaloy-2 Control Channels

b) Please provide measured creep data for NSF and Zry-2 at same temperature and differential pressure.

Response:

The measured creep bulge of NSF and Zircaloy-2 for the same channel design in the same plant type (i.e., similar differential pressures) is provided in Figure 2-11. The data indicate [[

]].

c) Describe the maximum ECBE and fluence for a GNF BWR channel under normal controlled operation throughout its lifetime (i.e., not suppressed).

Response:

The range of ECBE and exposure (an alternative to fluence) for the NSF channels in the GNF current database are provided in Figure A-5. This also is a reasonable representation of the range of ECBE and exposures in the Zircaloy-2 database. Maximum ECBEs can be as high as ~50,000 inch-days. More typically, the maximum ECBE value in a plant is between 20,000 and 35,000 inch-days. Discharge exposures typically range from the low 40s to the low 50s in GWd/MTU.

RAI-5 Channel Growth

Figure 2-13 of NEDE-33798P provides NSF and Zry-2 channel growth data, as well as NSF and Zry-2 irradiation growth data from BOR-60.

a) Correlate fluence to assembly average exposure for the NSF channel data.

Response:

The channel fluence plotted in Figure 2-13 is a weighted average of the axial fluence distribution. For the NSF channels, the average channel BWR fluence can be estimated as the product of [[ ]]*(exposure in GWd/MTU); this conversion factor is the average of the ratio of the NSF channel fluence to exposure for the data plotted in Figure 2-13. Thus, at 50 GWd/MTU the average BWR channel fluence is estimated as [[ ]] n/cm^2 and at 55 GWd/MTU (the estimated bundle average limit) the average BWR channel fluence is [[ ]] n/cm^2 or ~[[ ]] n/cm^2. However, because there is an axial distribution, the region around the center of the channel will have a higher fluence than the average.

b) Describe the irradiation conditions, particularly ECBE, for the NSF and Zry-2 channel growth data.

Response:

The growth data for Zircaloy-2 channels plotted in Figure 2-13 had ECBE values less than 4,500 inch-days; thus, the growth in these channels is attributed to only fluence-induced growth. For the NSF channels the data at ~4.5E21 n/cm^2 and ~9.0E21 n/cm^2 had ECBE values less than 4,500 inch-days; like the Zircaloy-2 channels the growth in these NSF channels is attributed to only fluence-induced growth. The NSF data at ~6.8E21 n/cm^2 had ECBE values of ~51,000 inch-days indicating a high susceptibility to shadow bow. Interestingly this data shows no bias in growth suggesting the majority of the length change is due to fluence-induced growth. This is also consistent with the observation of low shadow bow in these channels as shown in Figure A-9.

c) The maximum fluence reported for NSF channel data is about [[ ]] Please provide any data for NSF channels at higher fluences.

Response:

Two of the four channels operated to about 9.0E21 n/cm^2 were reinserted for a 4th cycle. These channels have been discharged but not yet inspected for channel distortion. One of the purposes of the 8% LUC program will be to provide more data in the higher fluence (i.e., exposure) region.

d) What is the expected maximum fluence for NSF channels in 6 and 8 years of operation?

Response:

As discussed in the response to Section (a) of this RAI, the maximum fluence in a channel will be in the region around the mid-elevation point. Because the growth of channels includes the entire distribution of fluences in the channel, the channel fluence is an average of this axial distribution. The bundle average exposure that corresponds to the [[ ]]. Using the correlation in the response to Section (a) of the RAI, the corresponding average channel BWR fluence would be ~[[ ]] n/cm^2. Again the maximum value of the fluence in this case will be higher than the average and probably ~[[ ]] n/cm^2.

e) Describe the difference in growth behavior between the NSF BOR-60 data and the NSF channel data.

Response:

The growth data from BOR-60 is a standard irradiation growth test where small coupons were irradiated, and the length was measured with an accurate Linear Variable Differential Transformer (LVDT)-type device. Because the BOR-60 is a fast reactor that has a different neutron energy spectrum than a BWR, the BOR-60 fluence (> 1 MeV) must be corrected to a BWR fluence (> 1 MeV). In addition, because of the size of the sample there is no fluence distribution in the sample.

The channel growth data is measured in the spent fuel pool with a calibrated tape measure and a video camera. In addition, there is a significant fluence distribution that is accounted for by using a weighted average calculation (as discussed above).

With these differences in sample and irradiation conditions, it is not surprising that there are differences in the absolute value of the growth. Rather the conclusion from the BOR-60 irradiation growth data is that NSF is resistant to breakaway growth. Also, while the NSF channel data is at a fluence that is near the predicted breakaway growth for Zircaloy, it is significantly lower than the comparable Zircaloy-2 channel growth data.

RAI-6 Calculating CPR with NSF Channels

a) Section A.2.2 of NEDE-33798P states, “Fast fluence (E>1MeV) gradient induced bow results from differential growth of channel material on opposite channel faces.” In Section 3.1.5, GNF states, “NSF channels do not bow significantly as a function of exposure, . . .”

i. Given that the data in Figure 2-13 show much the same growth behavior for Zry-2 and NSF channels, would not the differential growth be similar, and therefore the fluence-induced bow?

ii. Describe the magnitude of bow that would be considered "significant."

Response:

i. The data in Figure 2-13 show a significant difference in growth behavior between Zircaloy-2 and NSF. The Zircaloy-2 data clearly shows it is susceptible to breakaway growth while NSF is resistant to breakaway growth. In addition, the channel length data of NSF is significantly lower than the average Zircaloy-2 channel data at the same average fluence. Because fluence bow is a function of the growth rate and Zircaloy-2 exhibits a larger growth rate than NSF at fluences near breakaway, greater fluence bow is expected in Zircaloy-2 channels compared to NSF.

ii. "Significant" is a qualitative term that is not meant to invoke a quantitative number. Based on experience evaluating channel distortion in cells with channel-control blade interference, "significant" bow might be considered something greater than about 100 mils (as measured at the mid-elevation).

b) Figure 3-1 of NEDE-33798P provides calculated values of CACABO for 12 cycles of NSF cores.

i. For the data presented in Figure 3-1, please provide the channel type (e.g., 120/75, 100/60), the irradiation conditions for the calculated cases, including cell lattice (D, C, S), core power density, cycle length (EFPD) and ECBE at the beginning and end of the cycle. As part of the response, please indicate if the cycle is first, second, or third cycle.

ii. Please provide the CACABO values for a Zry-2 channel as a function of cycle exposure for Cycle F in Figure 3-1.

iii. Please provide the CACABO values for a Zry-2 channel as a function of cycle exposure for the case in Figure 3-1 with maximum ECBE.

Response

i. Table 6b-1provides the channel type, cell lattice, core power density, and cycle length for each of the cycles shown in Figure 3-1 of the LTR. Table 6b-2 shows Beginning-of-Cycle (BOC) and End-of-Cycle (EOC) ECBE values for each batch of fuel in each cycle from Figure 3-1. The LTR simulations included full cores of NSF channels (e.g., NSF channels on fresh, once-burnt, and twice-burnt fuel). Thus, the ECBE inch-days information is provided at BOC and EOC for each fuel batch.

Table 6b-1 Selected Plant Data for Plants in Figure 3-1 of the LTR

Plant Cycle	Channel Type	Lattice Type	Core Power Density [kW/L]	Cycle Length [EFPD]
Cycle A	[[	D	[[	[[
Cycle B		D		
Cycle C		D		
Cycle D		D		
Cycle E		D		
Cycle F		D		
Cycle G		C		
Cycle H		C		
Cycle I		S		
Cycle J		S		
Cycle K		D		
Cycle L	]]	D	]]	]]

Table 6b-2 ECBE at BOC and EOC for Each Fuel Batch

	Fresh Fuel Batch		2nd Cycle Batch		3rd Cycle Batch		4th Cycle Batch		5th Cycle Batch		6th Cycle Batch		7th Cycle Batch	
Plant Cycle	**BOC ECBE**	**EOC ECBE**	**BOC ECBE**	**EOC ECBE**	**BOC ECBE**	**EOC ECBE**	**BOC ECBE**	**EOC ECBE**	**BOC ECBE**	**EOC ECBE**	**BOC ECBE**	**EOC ECBE**	**BOC ECBE**	**EOC ECBE**
Cycle A	[[													
Cycle B														
Cycle C														
Cycle D														
Cycle E														
Cycle F														
Cycle G														
Cycle H														
Cycle I														
Cycle J														
Cycle K														
Cycle L														]]

ii. Figure 6b-1 shows the CACABO values as a function of exposure for a Zircaloy-2 core for Cycle F from Figure 3-1 in the LTR.

[[

]]

Figure 6b-1 CACABO Values for a Zircaloy-2 Core as a Function of Exposure for Cycle F from Figure 3-1 in the LTR

iii. Per Table 6b-2, Cycle C in Figure 3-1 from the LTR has the maximum ECBE value (fourth cycle batch). Figure 6b-2 shows the CACABO values as a function of exposure for a Zircaloy-2 core for Cycle C from Figure 3-1 in the LTR.

[[

]]

Figure 6b-2 CACABO Values for a Zircaloy-2 Core as a Function of Exposure for Cycle C from Figure 3-1 in the LTR

c) Figure A-6 of NEDE-33798P provides predicted versus measured fluence bow for NSF channels with ECBE < 4500 inch-days.

i. Please provide P vs M fluence bow data for NSF channels with ECBE > 4500 inch-days and M-P as a function of burnup (ref: Figures A-7 and A-8).

ii. Please provide the same data for corresponding Zry-2 channels, i.e., Zry-2 channels with the same or similar irradiation conditions to the same burnup and ECBE as the NSF channels.

iii. In equation A-17 of NEDE-33798P, a weighting factor 'f' is used in conjunction with the controlled time (i.e., time for which the control blade is inserted adjacent to the channel).

Please provide an example of how the weighting factor is used for cases where a channel is 1) controlled for two cycles, 2) controlled in the first cycle and uncontrolled in the second cycle, and 3) uncontrolled in the first cycle and controlled in the second cycle.

Response:

i. An updated version of Figure A-8 is provided in the response to RAI-6(d).

ii. The Measured-Predicted (M-P) data for Zircaloy-2 as a function of exposure for ECBE < 4,500 inch-days is provided on Slide 72 of MFN 12-134 (Reference 6-1). This data indicates the uncertainty around the prediction of fluence bow increases dramatically as a function of exposure for Zircaloy-2. The M-P Zircaloy-2 data for ECBE > 4,500 inch-days is plotted as inferred shadow bow vs. ECBE in RAI-9(c); inferred shadow bow is measured bow minus predicted fluence bow.

iii. The weight factor f is an effective control exposure weight, shown as a histogram in Figure 6c-1. It is dependent on the residence time of the channel (note: not the bundle, since in the case of re-channeling the two numbers are different). Its value is assigned based on the following histogram:

[[

]]

Figure 6c-1 Weighting Factors for Calculating Effective Control Blade Exposure (ECBE)

During operation, a sequence of control rods is used to control the core. Sequences are exchanged periodically in time to create a more uniform exposure distribution. During the first year, the weighting factor for the product between insertion distance and time (ECBE in units of inch-days) is [[ ]]. During the second year, the weighting factor is [[ ]]. During the third year, the factor decreases to [[ ]]. Beyond three years, ECBE does not accumulate. This calculation of ECBE weighs early-life control during the first two years much more significantly than control after two years.

d) Figure A-8 of NEDE-33798P provides M-P fluence versus exposure. On this figure, the data points for NSF channels with [[

]] What is the predicted and M-P fluence bow for NSF channels with ECBE > 4500 inch-days and exposure up to maximum approved burnup levels of GNF fuel assemblies?

Response:

Figure A-8 included all of the data collected as part of the LUC programs prior to January 2013. Since that date, seven NSF channels have been discharged and measured for distortion. These additional verified data have been added to Figure A-8, which is shown below in Figure 6d-1.

Data on higher burnup channels are planned to be measured and reported as part of the normal fuel performance update during the annual technology update meeting with the NRC.

[[

]]

Figure 6d-1 Redrawn Version of Figure A-8 in the NSF Channel LTR

Reference

6-1 Letter, A.A. Lingenfelter (GNF) to Document Control Desk (US NRC), "NSF Topical Report Pre-Submittal Presentation Slides," MFN 12-134, December 20, 2012.

RAI-7 Sample Calculation on Channel Bow

a) Please provide sample plots for bow (including FLUBOW, SHADBOW, CHANBOW, BOCELL, CACABO) of Zry-2 and NSF channels as a function of burnup for channels that exhibit different amounts of ECBE and different cycles of operation.

Response:

Background

Core-Average, Cell-Average Bow (CACABO) is a measure of the core-average channel bow and includes the contributions of

- Initial manufactured channel bow
- Fluence-induced channel bow
- Shadow corrosion-induced channel bow

Some nominal amount of channel bow is inherent to the manufacturing process; therefore, channels with no irradiation history (beginning of life channels) are still characterized by some amount of channel bow. Fluence-induced channel bow is caused by a fast fluence (E > 1MeV) gradient that results in differential growth of the channel material on opposite faces. Shadow corrosion-induced channel bow is an enhanced irradiation corrosion mechanism that occurs on zirconium alloys when a dissimilar material (such as a control blade) is near the zirconium surface (such as a BWR channel) and the water chemistry is oxygenated.

Calculation of CACABO and CACABO Uncertainty

[[

]]

To illustrate the different behavior of channel bow between Zircaloy-2 and NSF channels, nominal values of FLUBOW, SHADBOW, CHANBOW, and BOCELL are presented as part of this response.

Case Study of CACABO

A representative cycle design for a BWR/6 plant was chosen to provide an illustration of CACABO and its constituent contributors (including FLUBOW, SHADBOW, CHANBOW, BOCELL) to compare the behavior of Zircaloy-2 and NSF channels with different amounts of ECBE and different cycles of operation as a function of burnup.

The CACABO results of Zircaloy-2 and NSF channels are shown in Figure 7a-1. Note, the bundles that contribute to the calculation of CACABO [[

]]. The representative cycle design is one with a two-year cycle length. Both Zircaloy-2 and NSF results for CACABO are equivalent at the BOC, where CACABO is primarily influenced by [[

]]. The CACABO result for Zircaloy-2 channels begins at approximately [[ ]] mils and progressively increases to approximately [[ ]] mils at EOC. The CACABO result for NSF channels begins at approximately [[ ]] mils and slightly increases to approximately [[ ]] mils at EOC. The difference between the CACABO results of Zircaloy-2 and NSF channels as the cycle exposure increases is driven by fluence and shadow corrosion-induced channel bow, which will become more evident in the examination of FLUBOW and SHADBOW, respectively.

[[

]]

Figure 7a-1 Core-Average, Cell-Average Bow as a Function of Burnup (Cycle Exposure)

Five cells from the group of cells with at least one bundle that is defined as potentially limiting in bundle power were chosen to display BOCELL results of Zircaloy-2 and NSF channels. The characteristics of these five cells (ECBE, channel exposure, and channel residence time) are provided in Figure 7a-2 for both BOC and EOC. The BOCELL results of Zircaloy-2 and NSF channels are shown in Figure 7a-3 and Figure 7a-4. Figure 7a-3 shows results for cells with equivalent cell-average channel exposure and residence time but different amounts of ECBE. Figure 7a-4 shows results for cells with zero ECBE but different channel exposure and residence time. In general, the BOCELL results of the NSF channels are relatively constant as a function of cycle exposure. The BOCELL results of the Zircaloy-2 channels in Cells A and B exhibit the effects of high ECBE; whereas, the low accumulation of ECBE in Cell C is not significant. The BOCELL results of the Zircaloy-2 channels in Cells D and E exhibit break-away fluence-induced channel bow. Note, the changes in slope of the BOCELL results of the Zircaloy-2 channels (Cells A and D) are from the individual channels within the given cell either bowing (on average) toward or away from the control blade.

[[

]]

Figure 7a-2 Cell Characteristics for Select BOCELL Results

[[

]]

Figure 7a-3 Cell-Average Bow for Selected Cells A, B, and C as a Function of Burnup (Cycle Exposure)

[[

]]

Figure 7a-4 Cell-Average Bow for Selected Cells D and E as a Function of Burnup (Cycle Exposure)

Four channels from the group of bundles that contribute to CACABO were chosen to display CHANBOW, FLUBOW, and SHADBOW results of Zircaloy-2 and NSF channels. Note, the four channels do not belong to the five cells described above but were chosen based on different amounts of ECBE and different cycles of operation. The characteristics of these four channels (ECBE, channel exposure, and channel residence time) are provided in Figure 7a-5 for both BOC and EOC. The CHANBOW, FLUBOW, and SHADBOW results of Zircaloy-2 and NSF channels are shown in Figure 7a-6 and Figure 7a-7. Figure 7a-6 shows results for channels in their first cycle of residence and different amounts of ECBE. Figure 7a-7 shows results for channels in their second cycle of residence and different amounts of ECBE. Again, in general, the bow results of the NSF channels are relatively constant as a function of channel exposure. For channels in their first cycle of residence that have yet to reach the threshold for break-away fluence-induced channel bow, the FLUBOW results for both Zircaloy-2 and NSF channels are the same as shown in Figure 7a-6. Note, in Figure 7a-7, the total channel bow for Channel Y increases initially during the cycle from the accumulation of shadow corrosion-induced bow, but then decreases from fluence-induced bow after the shadow corrosion-induced bow becomes saturated.

[[

]]

Figure 7a-5 Channel Characteristics for Select CHANBOW, FLUBOW, and SHADBOW Results

In summary, NSF channels show much less sensitivity to fluence and shadow corrosion-induced channel bow than Zircaloy-2 channels, which explains the difference between the CACABO results of Zircaloy-2 and NSF channels.

[[

]]

Figure 7a-6 Total, Fluence-Induced, and Shadow Corrosion-Induced Channel Bow for Selected Channels W and X as a Function of Burnup (Channel Exposure)

[[

]]

Figure 7a-7 Total, Fluence-Induced, and Shadow Corrosion-Induced Channel Bow for Selected Channels Y and Z as a Function of Burnup (Channel Exposure)

b) In MFN 12-134, on page 72, GNF compares the measured-predicted (M-P) for fluence bow for NSF and Zr-2 channels. The NSF channels seem to have bounds on M-P of fluence bow of [[ ]] In another figure, Figure A-8 from the LTR, the M-P range [[ ]]

Pages 43-45 of MFN 12-134 mentions the uncertainty of channel bow is accounted for in the bundle R-factor calculation, and GNF states, [[
]]

On page 45 of MFN 12-134, GNF states (in NEDO-32601P), [[
]] With regard to FLN 2004-030, GNF indicates that [[
]]. These uncertainties apparently apply to Zr-2 channels.

Please provide a statement or explanation of how the R-factor uncertainty will be developed for and applied to NSF channels.

Response

The rod peaking and corresponding R-factor uncertainties in NEDC-32601P-A (Reference 7-1) were defined based on Zircaloy-2 channel bow characteristics. These uncertainties are conservative with respect to uncertainties that would result from similar studies that incorporated NSF channel bow considerations. For this reason, the continued application of these values is acceptable for assemblies with NSF channels.

To ensure further conservatism, the increase in R-factor uncertainty to [[ ]]% based on Zircaloy-2 shadow bow considerations described in FLN 2004-030 (Reference 7-2) will also continue to be applied for assemblies with NSF channels. As demonstrated in Section 3.1.5 of the LTR, calculations of BOWAVE uncertainties for NSF indicate that this increase may not be necessary. Any future reduction in R-factor uncertainty back to [[ ]]% to account for an NSF based BOWAVE uncertainty less than [[ ]] mils will be supported by measured data and justified in a transmittal to the NRC.

References

7-1 GE Nuclear Energy, "Methodology and Uncertainties for Safety Limit MCPR Evaluations," NEDC-32601P-A, August 1999.

7-2 Letter, John F. Schardt (GNF-A) to U.S. Nuclear Regulatory Commission Document Control Desk with attention to Mel B. Fields (NRC), "Shadow Corrosion Effects on SLMCPR Channel Bow Uncertainty," FLN-2004-030, November 10, 2004.

RAI-8 Measured and Predicted Bow

With respect to the Figure (M vs P, Limerick Lead Use Channel Inspections after 3rd cycle) on page 74 of MFN 12-134 (page 75 of 82 in pdf), please provide M vs P of bow for NSF LUC channels from Hatch 2 (Cycle 20-22) and Perry and Clinton.

Response:

The figure on page 74 is measured bow vs. predicted fluence bow for Zircaloy-2. This figure specifically highlights that NSF channels that experienced a fluence gradient that caused Zircaloy-2 channels to bow ~[[ ]] mil had only ~[[ ]] mil of fluence bow.

The measured vs. predicted NSF channel data are plotted in Figure A-6 for only the channels with ECBE values less than 4,500 inch-days. These channels are only susceptible to fluence gradient-induced bow. In Figure A-6, data from Limerick are provided. All the channels from Clinton and Perry (except from the most recent inspection in March 2015 that is yet to be verified) and most of the channels from Hatch Unit 2 had ECBE values greater than 4,500 inch-days. Figure A-6 shows that the model for fluence bow of NSF channels is reasonably predicting the nominal measured fluence bow.

RAI-9 Expanded Lead Use Channel Program

GNF proposed an expanded LUC program for NSF channels – MFN 12-074. The NRC approved the expanded program (March 29, 2013, ML13106A068).

a) Please provide an update on the status of current NSF LUA and expanded NSF LUC programs.

Response:

As background first consider the population of observations of interference in Figure 9a-1. The plant population is divided into plant types: S-Lattice, C-Lattice and D-Lattice. The important plant feature that effects channel control-blade interference is the gap distance between channel and control blade. The S-Lattice plants have the smallest gaps while the D-Lattice plants have the largest. Thus, the observations of interference followed the relative susceptibility to interference and first occurred in an S-Lattice plant, then C-Lattice, then D-Lattice. This same information is plotted per plant in Figure 9a-2. The plants listed in Figure 9a-2 provide the population of plants that have experienced channel control-blade interference with Zircaloy-2 and Zircaloy-4 channels.

As part of the current NSF LUC program and the expanded 8% LUC program, NSF channels are being inserted in a significant subset of the plants that have experienced interference (See Figure 9a-3). It is important to note that 8% quantities of NSF channels will be operating in all four S-Lattice plants in the US by the fall of 2015. Since the S-Lattice plants are the most susceptible to channel control-blade interference, any unexpected performance issues with NSF channels will be observed in this leading population and would enable the development of a mitigating response to full reloads inserted in 2016 and after.

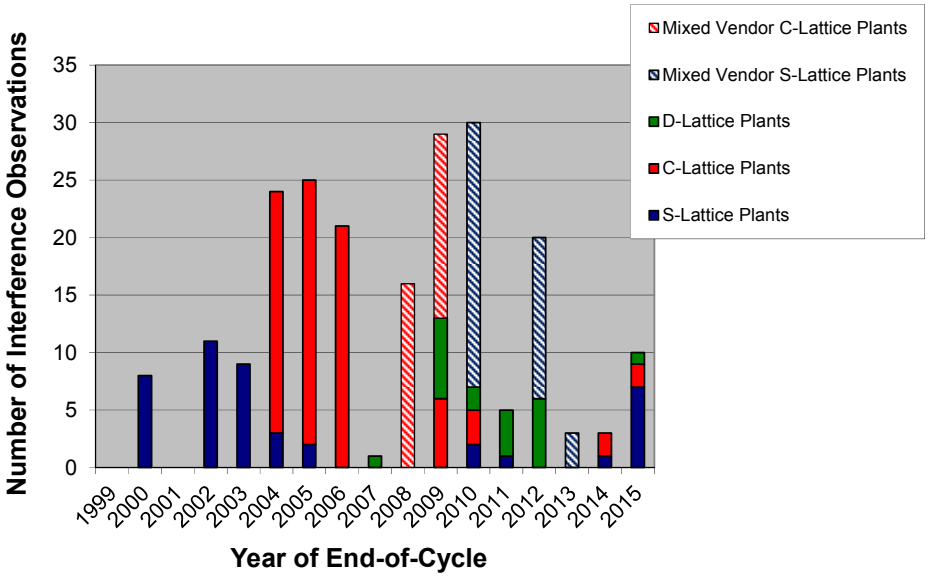

Figure 9a-1 Observations of a No-Settle Condition as a Function of the Year of End-of-Cycle

[[

]]

**Figure 9a-2 Observations of Interference in Specific Plants
(This provides the population of plants that have experienced channel control-blade interferences.)**

[[

]]

Figure 9a-3 The Plant Population Where NSF Channels Have Been or Will Be Inserted by the Fall of 2015

Below is a table (Table 9a-1) listing the plants where NSF channels have been inserted as part of normal LUC programs or as part of the expanded 8% LUC program. In 2014, GNF inserted [[ ]] Pre-Ox NSF channels, and in 2015, another [[ ]] will be inserted. Six US plants have inserted or will insert NSF channels as part of the expanded 8% LUC program.

Table 9a-1 History of NSF LUC and 8% Expanded LUC Programs

[[

]]

The following two tables summarize the conditions of the NSF channels that have been discharged and inspected (Table 9a-2) and the expected conditions of the NSF channels that will be discharged and inspected as part of the normal and 8% LUC programs (Table 9a-3). There will be a distribution in operating conditions with the majority of channels operating for ~six years (three two-year cycles); thus the majority of data will be collected in these conditions. In addition, the largest number of channels inspected after completion of the LUC programs will have operated in S-Lattice plants, which are most susceptible to channel interference. Operation into the 4th cycle is not universal. Where possible, NSF channels will be reinserted to operate out to near the [[ ]] residence time limit. Currently four NSF channels have operated for four two-year cycles.

Table 9a-2 Current NSF Database of Discharged and Inspected Channels as a Function of Plant Type, Exposure Range and Residence Time

[[

]]

Table 9a-3 Expected NSF Channel Database Once Channels Inserted by the Fall of 2015 are Discharged and Inspected (also as a function of plant type, exposure range and residence time)

[[

]]

b) Please provide the ECBE, EFPD and exposure (assembly burnup) for the channels in the following table.

Unit	Type - Lattice	Cycle Inserted	Number of Channels	Year Beginning	Year Discharge
[[					
					]]

Response:

Table 9b-1

Unit	Type - Lattice	Cycle Inserted	# of Channels	Years in Operation	Residence Time (days)	Exposure (GWd/MTU)	ECBE (in-days)
[[							
							]]

c) Update the figure below, Inferred Shadow Bow versus ECBE, with the latest data.

[[

]]

Figure MFN 12-134, p. 75 (76 of 82 in pdf)

Response:

[[

]]

Figure 9c-1

RAI-10 Future Surveillance / Reporting Program

The enhanced LUC program was approved to expedite data collection to support batch approval of NSF channels. Depending on the response to RAI-9 above, additional NSF in-reactor data may be necessary. In similar, past situations, the NRC has accepted a surveillance program which mandates data collection, confirmation of empirically-based models or performance, reporting requirements, and, where necessary, actions to ensure safe operation. The NRC has been willing to accept this approach when large quantities of lead use prototypes will continue to lead batch application such that compensatory action would be possible to avoid safety issues.

a) Please propose a surveillance program for the collection of NSF channel growth and distortion data and the confirmation of fluence gradient-induced bow and shadow corrosion-induced bow models. As part of this response, describe a process for updating models, implementing models, and reporting. The NRC is looking for assurance that existing fuel management guidelines, compensatory measures, and augmented control blade surveillances are not minimized prior to achieving high confidence NSF models.

Response

Monitoring Plan During Operation

The expanded NSF LUC program (Reference 10-1) includes provisions to ensure that NSF LUC channels are included in the normal plant Technical Specifications (TS) scram-time testing of 10% of the control rods every 120 days (nominally). Plants that have loaded NSF channels under the 8% LUC program will continue to monitor those channels based on the provisions of the LUC program. As discussed in the response to RAI-9, the population of plants where NSF has been inserted under the 8% LUC program is representative of the plants that have experienced channel control-blade interference (including all four BWR/6, S-Lattice plants in the US). However, when reload quantities of NSF are loaded into the core, the probability of scram-time testing cells with NSF channels is greatly increased such that the specific provisions of the LUC program for added scram-time testing are no longer needed to ensure NSF channels are adequately included in the tested population.

If there is a friction observation in a cell, the plant will immediately go into MFN 10-245 R6 (Reference 10-2) or MFN 08-420 R1 (Reference 10-3) testing. For plants transitioning to full core use of NSF channels, the friction monitoring provisions of References 10-2 and 10-3 will continue to apply. That is, these procedures will remain in place to manage any potential unforeseen channel distortion issues with NSF. However, the expectation is that as plants transition to 100% NSF there will be no observations of channel–control blade interference.

Post-Irradiation Surveillance Plan

The 8% LUC program requires that a subset [[ ]] of the expanded NSF LUC program channels be inspected visually to evaluate corrosion performance and to measure the length change. Further, after discharge, a subset [[ ]] of the expanded NSF

LUC program channels will be [[
]]. In addition after discharge, [[
]] of the NSF LUC channels to confirm that [[
]]. This program will continue on channels introduced via the 8% LUC program.

A total of more than 300 channels will be inserted into six plants as part of the 8% LUC program representing operation in all plant lattice types (D-, C- and S-Lattice) and both the thick and thin channel designs. In addition, there are 28 NSF channels operating in four US plants as part of the normal 2% LUC program. This population of channels represents a good cross section of variations in channel material within the specification range and operational experience and will lead the reload quantities by at least one two-year cycle. Per the inspection requirements, channel distortion measurements will be performed on approximately 225 NSF channels; the expected range of conditions in this measurement population was provided in the response to RAI-9 (see Table 9a-3). Because these lead channels are being placed in aggressive locations relative to the mechanics of channel distortion, the experience and measurements from these channels alone will provide sufficient evidence for the observed variability in the distortion of NSF channels and confirm the fluence gradient-induced bow and shadow corrosion-induced bow models. In addition to the channel visual, length, and distortion measurements, GNF will measure oxide thickness using a non-destructive, pool-side technique or alternative method on ~20 high exposure bundles (~6 and ~8-year residence time) to confirm the oxide thickness design curve in Figure 2-12. As the full reloads of NSF channels are discharged, inspections of channel distortion will only occur as is deemed necessary.

Reporting

GNF will provide a progress report to the NRC each year on the inspection program results for both the 8% LUC program and the requirements as described in the NSF LTR.

When the post-irradiation surveillance protocol is complete, GNF will provide an information report to the NRC summarizing the results. It is anticipated that the proposed fluence gradient-induced bow and shadow corrosion-induced bow models will be confirmed and will not require modification.

In the unlikely event that changes to the fluence gradient-induced bow and shadow corrosion-induced bow models are necessary, GNF will evaluate the impact on the process for calculating the Critical Power Ratio (CPR) defined in the NSF LTR and communicate the results of that evaluation to the NRC in an information letter.

b) Similar to above, for the core-average, cell-average bow input to the channel-bow dependent critical power ratio calculation.

Response

The recommendation in the NSF LTR is to use a [[ ]] for the core-average, cell-average bow for NSF channels. This recommendation is based on the observation that [[ ]] (Figure 3-1 in the LTR). These predictions are based on the channel bow models provided in Appendix A. As discussed above in the section on the Post Irradiation Inspection Plan, channel bow will be measured on approximately 225 NSF channels to confirm the channel bow models. If the channel bow data collected on NSF indicates a need to modify the channel bow models, the impact on the prediction of core-average, cell-average bow will be evaluated and communicated to the NRC.

References

10-1 Letter, A.A. Lingenfelter (GNF) to Document Control Desk (US NRC), "Accepted Version of Enhanced Lead Use Channel (LUC) Program for NSF Fuel Bundle Channels," MFN 12-074 Supplement 2-A, April 15, 2013.

10-2 Letter, D. E. Porter (GEH) to Document Control Desk (US NRC), "Update to Part 21 Reportable Condition Notification: Failure to Include Seismic Input in Channel-Control Blade Interference Customer Guidance," MFN 10-245 R6, December 16, 2013.

10-3 Letter, D. E. Porter (GEH) to Document Control Desk (US NRC), "Update to GEH Surveillance Program for Channel-Control Blade Interference Monitoring," MFN 08-420 R1, December 16, 2013.